Mobility Modeling Considerations for Radiation Effects Simulations in Silicon

Daniel J. Cummings, *Student Member, IEEE*, Arthur F. Witulski, *Senior Member, IEEE*, Hyunwoo Park, *Student Member, IEEE*, Ronald D. Schrimpf, *Fellow, IEEE*, Scott E. Thompson, *Fellow, IEEE*, and Mark E. Law, *Fellow, IEEE*

***Abstract*—The results of semiconductor device simulations are highly dependent on the electron and hole mobility models. The manner in which mobility is modeled at high-injection levels is especially important for single-event upset simulations due to the large number of electron-hole pairs generated along a particle strike path. This paper presents an approach to modeling mobility that describes majority and minority carrier mobility, carrier-carrier scattering, and temperature dependence in a computationally efficient form relevant for radiation effects simulations in silicon.**

***Index Terms*—Carrier-carrier scattering, device simulation, mobility model, radiation effects, single-event upset.**

I. Introduction

THE simulation of radiation effects is an increasingly important area of numerical device simulation since the sensitivity of microelectronics to single-event upset (SEU) is expected to increase as technology scaling continues [1]. For example, high-energy heavy ions, alpha particles, protons, or secondary particles produced by neutron interactions can cause changes in memory state due to the resulting charge collection. Consequently, as devices are down-sized, a reduction in the amount of charge held on storage nodes increases device vulnerability to SEU [2]. Device simulations are a useful way to predict and interpret device behavior for such conditions, since comprehensive experimental testing for all particles, angles, and energies of interest is impractical.

The characteristics of semiconductor devices are modeled by three coupled nonlinear partial differential equations consisting of the electron continuity, hole continuity, and Poisson equations. The results of semiconductor device simulations are highly dependent on the electron and hole mobility models. For instance, the overall effect of mobility on current density can be shown in terms of quasi-Fermi levels as

$$J_n = -q\mu_n n \nabla \phi_n \tag{1}$$

$$J_p = -q\mu_p p \nabla \phi_p \tag{2}$$

where n and p are the electron and hole densities, $\phi_{n,p}$ the quasi-Fermi levels, $J_{n,p}$ the current density and $\mu_{n,p}$ the mobilities. Therefore, it is important to choose an accurate mobility model so that the simulation results will be relevant. The manner in which mobility at high injection levels is modeled is especially important since a large number of electron-hole pairs are generated along a particle strike path [3]. Since a particle strike generates an equal number of free holes and electrons, the mobility is qualitatively important because it affects how rapidly and how far the deposited charges separate, and hence has a first order effect on the potential distribution and charge collection during the strike recovery.

Because a large number of mobility models have been formulated for various purposes and are available for device simulation, a brief comparison between these existing models is presented. While most mobility models emphasize inversion-layer transport, for radiation effects simulations, bulk mobility is more important because high-injection conditions occur into the depth of the device away from interfaces. Due to inconsistencies between existing bulk models and experimental data, an alternative approach to modeling mobility is presented. The proposed mobility model accounts for majority and minority carrier mobility, carrier-carrier scattering, and temperature dependence in a computationally efficient form.

II. Mobility Model Comparison

Due to the large number of free carriers that exist in the substrate immediately following a particle strike, it is important to model carrier mobility in the bulk of the device. For radiation effects simulations, various bulk mobility models for device simulation are available, each with particular advantages [4]–[8]. Some models focus on the accurate fitting of mobility versus doping levels, whereas other models focus on temperature dependence and so on. A summary of conventional bulk mobility models is given in Table I. Each model is qualitatively compared against others with respect to majority carrier mobility, minority carrier mobility, carrier-carrier scattering, and temperature dependence. For example, the Masetti model can be used for its

Manuscript received November 17, 2009; revised April 07, 2010 and June 03, 2010; accepted June 07, 2010. Date of current version August 18, 2010. This work was supported by the Air Force Office of Scientific Research (AFOSR) through the MURI program.

D. J. Cummings, H. Park, S. E. Thompson, and M. E. Law are with the Department of Electrical and Computer Engineering, University of Florida, Gainesville, FL 32611 USA (e-mail: danieljc@ufl.edu; hwpark76@ufl.edu; thompson@ece.ufl.edu; law@tec.ufl.edu).

A. F. Witulski and R. D. Schrimpf are with the Department of Electrical Engineering and Computer Science, Vanderbilt University, Nashville, TN 37235 USA (e-mail: art.witulski@vanderbilt.edu; ron.schrimpf@vanderbilt.edu).

Color versions of one or more of the figures in this paper are available online at http://ieeexplore.ieee.org.

Digital Object Identifier 10.1109/TNS.2010.2052831

TABLE I
QUALITATIVE COMPARISON OF COMMONLY USED BULK SILICON MOBILITY MODELS FOR DEVICE SIMULATION

Parameter / Model	Majority Carrier Mobility	Minority Carrier Mobility	Carrier-Carrier Scattering	Temperature Dependence
Proposed	+	+	+	+
Philips [4]	+	+	-	+
Dorkel [5]	-	n/a	+	-
Masetti [6]	+	n/a	n/a	n/a
Arora [7]	-	n/a	n/a	+
Caughey [8]	-	n/a	n/a	n/a

\+ Accurate model fitting to experimental data
\- Loose approximation to experimental data
n/a Not available in model

excellent fitting to majority carrier data but lacks a carrier-carrier scattering description, limiting its applicability in situations with high carrier densities, e.g., following an ion strike [6].

An important aspect of radiation effects simulations is how the mobility model treats high-injection electron-hole carrier densities. As pointed out by Dodd [3], the charge densities immediately after the passage of an ionizing particle can exceed 10^{20} cm^{-3}. For carrier densities below 10^{18} cm^{-3}, Dannhauser [9] and Krausse [10] measured the sum of electron and hole mobilities as a function of the concentration of carriers injected into the weakly doped region of a silicon P-I-N diode. Unfortunately, very little experimental data has been published for electron-hole carrier densities above 10^{18} cm^{-3}. Although limited data are available, approximations based on semi-classical quantum theory, such as the Conwell-Weisskopf or Brooks-Herring models, predict that an increase in electron and hole density results in a decrease in carrier mobility [11]. Two bulk mobility models that account for carrier-carrier scattering are the Philips unified mobility model and the Dorkel-Leturcq mobility model.

The Philips unified mobility model is a commonly used mobility model for device simulation and has been used for recent simulation work in the area of CMOS and SiGe HBT radiation effects [12], [13]. The Philips model accounts for majority and minority carrier mobility, the screening of the impurities by charge carriers, electron-hole scattering, clustering of impurities, and temperature dependence [4]. However, the carrier-carrier scattering in the Philips model is formulated in such a way such that it does not match known experimental data for electron and hole concentrations above 10^{17} cm^{-3}. Therefore, TCAD simulations result in single event current pulses that are too large when using the Philips model, and hence voltage pulse-widths that are too short as discussed in [3].

For single event simulations, the Dorkel-Leturcq model has been suggested as a better alternative to the Philips model since at high electron-hole densities, the mobility agrees better with measured data [14]. This model describes mobility in terms of doping dependence and carrier-carrier scattering. However, for modern devices it lacks accurate majority and minority mobility descriptions since the model was primarily designed for doping levels below 10^{19} cm^{-3} [5]. Also, a disadvantage of the Dorkel-Leturcq model is that it does not fit the data well at high doping concentrations and has not been formulated for minority carrier mobility.

III. PROPOSED MOBILITY MODEL

The goal of this work is to formulate a mobility model suitable for radiation effects simulations that accurately describes majority and minority carrier mobilities, carrier-carrier scattering, and temperature dependences. There are several ways to approach the modeling of mobility. Some methods formulate mobility starting from fundamental quantum mechanics principles and therefore are very computationally intensive [15]. Other mobility modeling methods start with simplified formulations of lattice and ionized impurity scattering and then use fitting parameters to match experimental data [4]–[8]. Our proposed mobility model uses the latter approach to modeling mobility since computational efficiency is important for device simulations. As discussed in the following sections, the proposed model combines the most accurate dependencies (e.g., doping levels, temperature, carrier-carrier scattering) from existing mobility models to form a single mobility model set suitable for radiation effects device simulations in silicon.

A. Majority Carrier Modeling

The majority carrier modeling in this section describes the lattice scattering and ionized impurity scattering processes of electrons in n-type material and holes in p-type material. To formulate the majority carrier mobility for the proposed model, the well-defined doping and temperature functions in the Masetti and Arora models will be combined. The mobility derivation is best understood by starting with the modeling approach of Caughey-Thomas which shows that plots of experimentally measured mobility data versus the logarithm of doping density strongly resemble the Fermi-Dirac function [8]. The Caughey-Thomas mobility model in terms of doping density is expressed as

$$\mu = \mu_{\min} + \frac{\mu_{\max} - \mu_{\min}}{1 + (N/C_{\text{ref}})^{\alpha}} \tag{3}$$

where C_{ref} and α are fitting parameters, N is the total doping density, and $\mu_{\min}$ and $\mu_{\max}$ describe the "min-max" behavior of the function. The above model is suitable for lower impurity concentrations but is inaccurate at higher concentrations. Building upon (3), a third term is added to account for the additional decrease in mobility that occurs when the doping level is more than 5×10^{19} cm^{-3} [6]. This results in the Masetti mobility model and is of the form

$$\mu = \mu_0 + \frac{\mu_{\max} - \mu_0}{1 + (N/C_{\text{ref},1})^{\alpha_1}} - \frac{\mu_1}{1 + (C_{\text{ref},2}/N)^{\alpha_2}}. \tag{4}$$

The Masetti model is shown in Figs. 1 and 2 where it is compared against the Dorkel-Leturcq, Philips and proposed mobility models. The Masetti model has been fitted to experimental data very accurately for both electrons and holes since majority carrier mobility has been heavily investigated. The parameters for

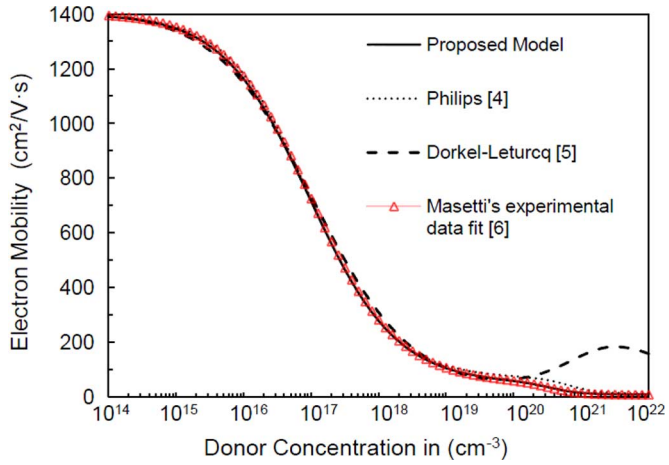

Fig. 1. Majority electron mobility as a function donor concentration for different mobility models at 300 K.

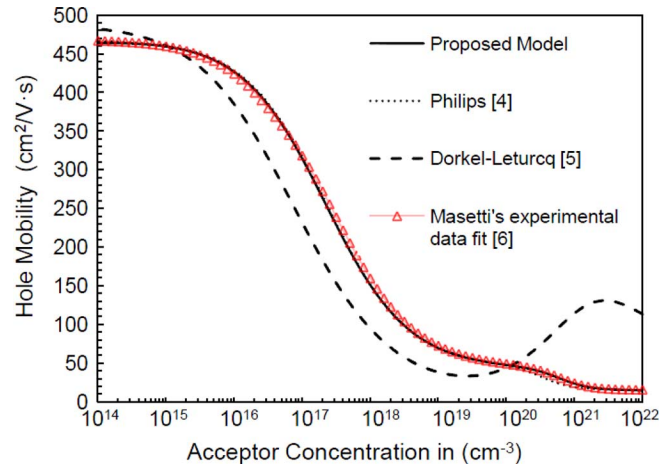

Fig. 2. Majority hole mobility as a function of acceptor concentration for different mobility models at 300 K.

TABLE II
MAJORITY CARRIER MOBILITY FITTING PARAMETERS*

Parameter	Electrons (in n-type Si)	Holes (in p-type Si)
μ_{max}	1417	470.5
μ_0	52.2	44.9
μ_1	39.4	29.0
α_1	0.68	0.719
α_2	2.0	2.0
$C_{ref,1}$	$9.68 \cdot 10^{16}$	$2.23 \cdot 10^{17}$
$C_{ref,2}$	$3.43 \cdot 10^{20}$	$6.10 \cdot 10^{20}$

*The fitting terms are given for the case of 300 K. The parameters for electrons assume the n-type dopant is arsenic. Parameters for phosphorus are available in [6].

the majority carrier mobility are given in Table II and are based on [6].

A disadvantage of the Masetti formulation is that it is not a function of temperature. To add temperature dependence, the Arora mobility model approach is used since it is well fit to experimental data with mobility as a function of temperature [7]. The Arora model can be formulated in terms similar to the Caughey-Thomas expression in (3) where the terms $\mu_{\min}$, $\mu_{\max}$, C_{ref} and α can be written as functions of temperature [7], [16].

TABLE III
TEMPERATURE DEPENDENCE FITTING PARAMETERS

Parameter	Electrons	Holes
γ_0	-0.57	-0.57
γ_1	-2.33	-2.33
γ_2	2.4	2.4
γ_3	-0.4	-0.4
γ_4	-2.33	-2.8

Using the same approach, but building on the Masetti formulation in (4), the new proposed majority carrier mobility can be written as

$$\mu_{i,\text{maj}} = \mu_0 T_n^{\gamma_0} + \frac{(\mu_{\max} - \mu_0)\, T_n^{\gamma_1}}{1 + \left(\frac{N}{C_{\text{ref},1} T_n^{\gamma_2}}\right)^{\alpha_1 T_n^{\gamma_3}}} - \frac{\mu_1}{1 + \left(\frac{C_{\text{ref},2}}{N}\right)^{\alpha_2}} \quad (5)$$

where $T_{\text{n}} = (T/300\,\text{K})$. The subscript i stands for e (electrons) or h (holes) and the T_{n}^{γ} terms are the temperature fitting parameters. The third term on the right hand side of (5) is not a function of temperature since for high impurity concentrations, the carrier mobility in silicon becomes nearly temperature independent [17]. The values for the temperature fitting parameters are given in Table III. The parameters are based on Arora's model but are modified to fit the experimental temperature data in [17]–[19].

A comparison between the proposed model, the Arora model, and measured data for both electron and hole mobilities is given in Figs. 3 and 4. The plots show that both models follow a similar mobility trend over a range of temperatures. Since the Arora model uses a formulation based on Li and Thurber [17] and the proposed model follows Masetti [6], a small difference in results is observed. For doping levels higher than 10^{19} cm^{-3}, the proposed model fits experimental data better since the Arora model over-predicts mobility at high doping levels.

B. Minority Carrier Modeling

Minority carrier mobility is a description of the scattering processes of electrons in p-type material and holes in n-type material. As with the majority carrier formulation in the previous section, a similar approach is used to model the minority carrier mobility by using the Caughey-Thomas and Masetti expressions as a starting point. Because the Masetti model does not include minority carrier mobility (Table I), a new set of fitting parameters is used. Following the temperature dependence approach in (5), the new proposed formulation for minority carrier mobility is of the form

$$\mu_{i,\min} = \mu_0 T_n^{\gamma_0} + \frac{(\mu_2 - \mu_0)\, T_n^{\gamma_4}}{1 + \left(\frac{N}{C_{\text{ref},3} T_n^{\gamma_2}}\right)^{\alpha_1 T_n^{\gamma_3}}} - \frac{\mu_3}{1 + \left(\frac{C_{\text{ref},4}}{N}\right)^{\alpha_2}} + \mu_{\text{fit}} \quad (6)$$

where μ_{fit} is an additional fitting term. The fourth term on the right hand side of (6) arises from the fact that experimental data

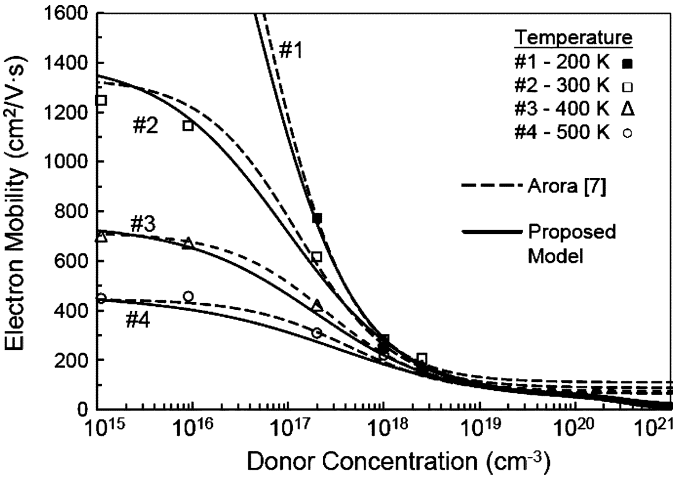

Fig. 3. Majority electron mobility as a function of temperature and donor concentration. Symbols represent experimental data from [17].

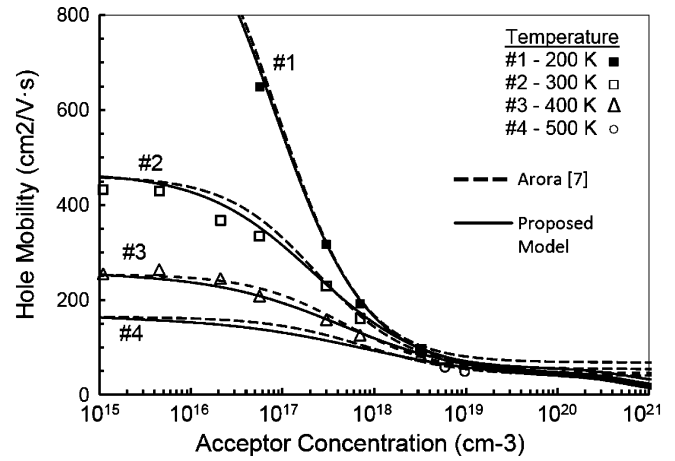

Fig. 4. Majority hole mobility as a function of temperature and acceptor concentration. Symbols represent experimental data from [18], [19].

show that minority carrier mobility exceeds majority carrier mobility at high doping concentrations ($\sim 1\times10^{18}-1\times10^{20}\,\mathrm{cm}^{-3}$) [20]. This additional fitting term for the majority and minority difference is formulated as

$$\mu_{\mathrm{fit}} = \frac{\mu_4}{1+(C_{\mathrm{ref},5}/N)^{\alpha_4}}. \tag{7}$$

and behaves like a sigmoid function. As with the majority carrier mobility, the last two terms in (6) are not functions of temperature and are only used for fitting high impurity concentration data. It should be noted that no extensive experimental data on the minority-carrier mobility as a function of temperature is available, according to Klaassen [20]. Therefore, the temperature fitting parameters were set such that the minority-carrier mobility of the proposed model follows the trend of the Philips minority-carrier mobility model. The additional parameters required for fitting the minority-carrier data are listed in Table IV.

The mobility model in (6) is compared to experimental data and the Philips model in Figs. 5 and 6. The comparison is made against the Philips model since it is well formulated for minority-carrier mobility. The trend of the proposed model is in agreement with the Philips mobility model for both electron and hole-minority carrier mobilities.

TABLE IV
MINORITY CARRIER MOBILITY FITTING PARAMETERS*

Parameter	Electrons (in p-type Si)	Holes (in n-type Si)
μ_2	1270	370
μ_3	39	33
μ_4	150	100
$C_{\mathrm{ref},3}$	$4.68\cdot10^{16}$	$1\cdot10^{17}$
$C_{\mathrm{ref},4}$	$3.34\cdot10^{20}$	$3.34\cdot10^{20}$
$C_{\mathrm{ref},5}$	$2\cdot10^{20}$	$2\cdot10^{20}$
α_4	3.7	3.7

*The parameters in this table are used in conjunction with parameters given in Tables II and III.

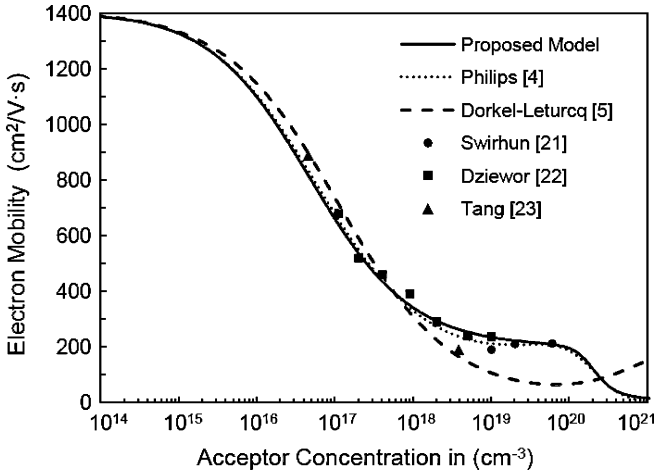

Fig. 5. Minority electron mobility in p-type silicon at 300 K. Symbols represent experimental data from [21]–[23].

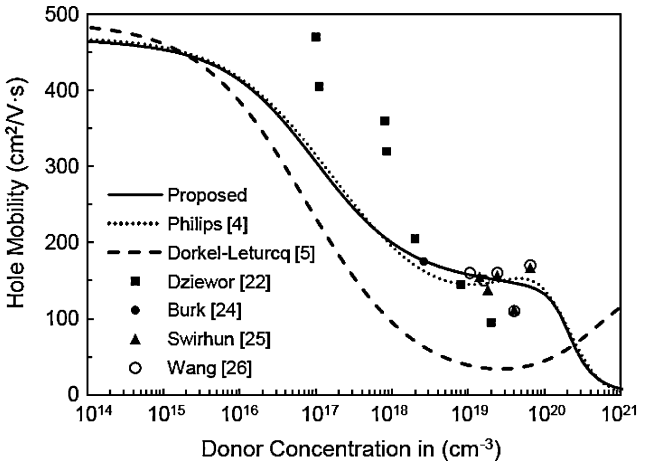

Fig. 6. Minority hole mobility in n-type silicon at 300 K. Symbols represent experimental data from [22], [24]–[26].

In order for the majority and minority mobilities to be continuous functions, Mathiessen's rule is used with a simple ratio term. Using (5) and (6), the mobilities for electrons and holes can be written as the following set of equations

$$w = N_D/(N_D+N_A) \tag{8}$$

$$\mu_{e,\mathrm{dop}} = \left(\frac{w}{\mu_{e,\mathrm{maj}}} + \frac{1-w}{\mu_{e,\mathrm{min}}}\right)^{-1} \quad (9)$$

$$\mu_{h,\mathrm{dop}} = \left(\frac{1-w}{\mu_{h,\mathrm{maj}}} + \frac{w}{\mu_{h,\mathrm{min}}}\right)^{-1}. \quad (10)$$

where w is the dopant ratio that allows for the continuous transition between the majority and minority carrier mobilities. Thus mobility as a function of doping levels has been formulated where $\mu_{\mathrm{e,dop}}$ defines the electron mobility and $\mu_{\mathrm{h,dop}}$ defines the hole mobility.

C. Carrier-Carrier Scattering

For radiation effects, the carrier-carrier scattering effect becomes very important due to the high amount of electron-hole pairs that are generated in the device during a particle strike. In order to account for carrier-carrier scattering, a modified expression of the Conwell-Weisskopf formula proposed by Choo [27] is used and is of the form

$$\mu_{\mathrm{cc}} = \frac{1.04 \times 10^{21} T_n^{3/2}}{\sqrt{np}} \times \left[\ln\left(1 + 7.45 \times 10^{13} T_n^2 (pn)^{-1/3}\right)\right]^{-1} \quad (11)$$

where n and p are electron and hole densities in cm^{-3}. The doping dependent mobility and carrier-carrier scattering mobility terms are combined using the Mathiessen formula as

$$\mu_{i,b} = \left[\frac{1}{\mu_{i,\mathrm{dop}}} + \frac{1}{\mu_{\mathrm{cc}}}\right]^{-1} \quad (12)$$

where the subscript i stands for e or h. This results in a unified term for bulk mobility that is a function of doping levels, electron and hole densities, and temperature. The effect of carrier-carrier scattering in (12) is compared against experimental data in Fig. 7. As previously discussed, the Philips model highly overestimates mobility at electron-hole levels over 10^{17} cm^{-3}. In contrast, the Dorkel-Leturcq model uses a similar approach to carrier-carrier scattering as the proposed model. The Dorkel-Leturcq model fits well for lower carrier concentrations but at concentrations of more than 10^{17} cm^{-3}, begins to under-predict mobility. Another issue is that at high-injection levels of more than 5×10^{19} cm^{-3}, the Dorkel-Leturcq model predicts a negative mobility and thus requires an arbitrary minimum mobility condition to be enforced [3].

In comparison to experimental data, the proposed model only slightly overestimates the mobility at lower concentrations. However, the electron-hole pair concentration generated by a particle strike is typically very high (more than 10^{17} cm^{-3}) [3]. For this important region, the proposed model continues on the assumption that an increase in electron and hole density results in a decrease in carrier mobility [27]. Above a carrier concentration of 10^{17} cm^{-3}, the proposed model predicts a mobility between the Philips and Dorkel-Leturcq models and eventually converges to $\sim$2 cm^2/V·s at a carrier concentration of 10^{22} cm^{-3}.

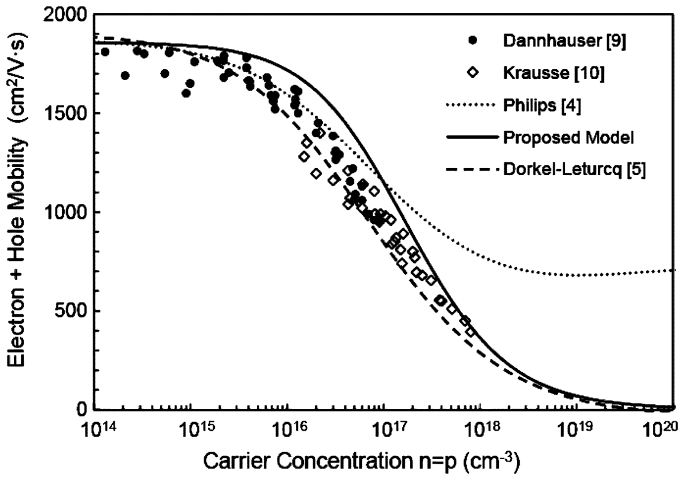

Fig. 7. Sum of electron and hole mobility as a function of carrier concentration versus experimental data at 300 K. Symbols represent experimental data from [9], [10].

Many complications arise when modeling carrier-carrier scattering for the ultra high-injections conditions that occur following a particle strike. For example, carrier concentrations become degenerate requiring the use of Fermi-Dirac statistics, carrier kinetic energies increase, and ambipolar diffusivity increases [28]. Some work has theorized that because carriers are moving together due to ambipolar transport, carrier-carrier scattering may be minimized suggesting that classical scattering models may not apply for high-injection situations [29]. Also, thermalization in the lattice and bandgap narrowing can be factors [30]. Due to these and other complexities, the experimental data shown in Fig. 7 serves as a reminder that more data are needed for carrier concentrations above 10^{18} cm^{-3}.

D. Transverse Field and High-Field Saturation

For devices such as MOSFETs, acoustic phonon scattering and surface roughness scattering dominate the mobility at the channel interface whereas the bulk mobility dominates in low field regions away from the inversion layer. Models for the degradation of mobility at interfaces have been well formulated by Lombardi [31] and Darwish [32]. In these approaches, the transverse field $E_\perp$ dependent mobility terms are combined with the bulk mobility term using the Mathiessen rule as

$$\mu_0 = \left[\frac{1}{\mu_b} + \frac{1}{\mu_{\mathrm{ac}}(E_\perp)} + \frac{1}{\mu_{\mathrm{sr}}(E_\perp)}\right]^{-1} \quad (13)$$

where μ_{b} represents the bulk mobility formulated in (12), μ_{ac} the acoustic phonon scattering, and μ_{sr} the surface roughness scattering. Since the interface models are already very well fit to experimental data, the mobility defined in (13) is used as given in [32]. To account for high-field saturation, the Canali [33] approach can be used and is formulated as

$$\mu(E_\parallel) = \frac{\mu_0}{\left[1 + \left(\frac{\mu_0 E_\parallel}{v_{\mathrm{sat}}}\right)^{\beta}\right]^{1/\beta}} \quad (14)$$

TABLE V
OVERVIEW OF THE SIMULATION VARIABLES

Simulation Set	Set 1	Set 2	Set 3
Comparison to experiment data	Yes	No	No
Structure type	N^+/P diode [34]	N^+/P diode [34]	Epitaxial N^+/P diode [37]
Generated electron-hole pair profile	Single-Photon Absorption [36] Energy=13.5 pJ	Gaussian LET = 20 MeV-cm^2/mg	Gaussian LET = 20 MeV-cm^2/mg

where μ_0 is the low field mobility, $E_{||}$ is the driving field, β is a temperature dependent fitting parameter. The Canali model also is based on the Caughey-Thomas formula as in (3) and is commonly used in device simulation programs [16], [33].

IV. SIMULATION RESULTS AND DISCUSSION

A series of three-dimensional single-event transient simulations were run to compare the results obtained using the proposed mobility model to those obtained from the Philips and Dorkel-Leturcq models. The first set of simulation results was also compared to experiments performed by Park *et al.* [34]. The simulation tool used for this study is the Florida object oriented device simulator (FLOODS) [35]. The three mobility models compared in the simulations are the Philips model, the Dorkel-Leturcq model, and the proposed model. A minimum mobility condition (2 cm^2/V.s) is applied to the Dorkel-Leturcq model to prevent the mobility from going negative, as previously discussed. In addition to these three models, a constant mobility model ($\mu_e = 1417$, $\mu_h = 470.5$ cm^2/V·s) is used to show what occurs when only phonon scattering is considered [33].

Three different sets of simulations were run to compare the mobility models. In the first set, the mobility models were compared for a 13.5 pJ laser-induced current transient and are compared to experimental results (pulsed lasers are frequently used to create conditions similar to those produced by an ion strike) [34]. Since the experiment only reached injection levels of 9.8×10^{17} cm^{-3}, two additional sets of simulations were performed to provide insight into the effects of higher injection levels. For the second and third simulation sets, the carrier generation was modeled using a cylindrically symmetrical Gaussian profile more similar an ion strike track. The second set uses the same N^+/P diode structure as the experiment. For third set, an epitaxial (EPI) N^+/P^+ diode structure was simulated. The simulation variations are summarized in Table V. The dimensions of width, length and depth for the simulation structures were $30 \times 30 \times 40$ μm and were large enough to minimize reflection at the boundaries (Fig. 8). For each simulation, the velocity saturation model in (12), Shockley-Read-Hall recombination and Auger band-to-band recombination models were used.

A. Experiment Setup

Laser-induced current transients on Si N^+/P junction diodes were reported in [34]. The diodes were fabricated on (001) Si wafers using 130-nm process technology. The diode structure consisted of a heavily doped n^+ region (10^{20} cm^{-3}) in a p-well (10^{18} cm^{-3}) that resolved into a p-type substrate (10^{16} cm^{-3}). The n^+ and p-well junction depths were 0.1 μm and 1.5 μm, respectively, and a 5 V reverse bias was applied to the device. In the experiment, a cavity-dumped dye laser with a wavelength of 590 nm and a pulse width of 1 ps was used to generate electron-hole pairs in the diode (Fig. 8). The laser direction was normally incident to the diode surface, had a spot size of 12 μm in diameter and the energy reaching the active area of the diode was 13.5 pJ [34].

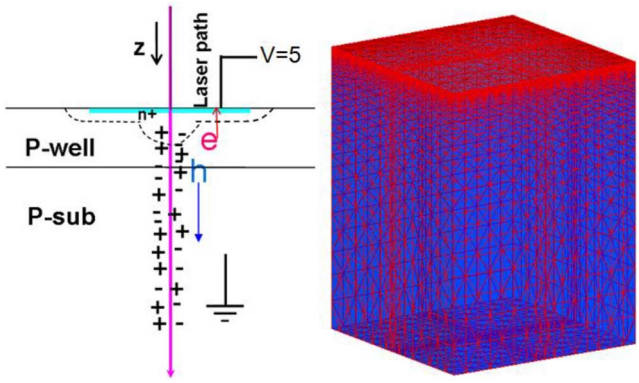

Fig. 8. Schematic of laser-induced current transients [34] and 3-dimensional simulation structure of the N^+/P diode, $30 \times 30 \times 40$ μm.

B. Generated Carrier Distribution

For the first simulation set, the number and distribution of N electron-hole pairs generated by the laser pulse was calculated by using the single-photon absorption (SPA) equation developed by McMorrow [36]. In this model, N as a function of depth in Si is described by:

$$N_{1P}(z) = \frac{\alpha}{\hbar\omega} \exp(-\alpha z) \int_{-\infty}^{\infty} I_o(z,t)dt \qquad (15)$$

where α is the absorption coefficient of Si, $\hbar\omega$ is the photon energy (2.1 eV), z is depth in the Si, I_0 is the intensity of the laser beam, and t is the time. For the second and third simulation sets, the generated electron-hole pairs were modeled using a cylindrically symmetrical Gaussian profile. The Gaussian profile had a $1/e$ radius of 50 nm, terminated at a depth of 30 μm, and had a linear energy transfer (LET) value of 20 MeV-cm^2/mg. Fig. 9 shows the carrier distribution for the SPA model in (15) and the cylindrical Gaussian profile. The maximum carrier concentrations for the SPA and Gaussian profiles were 9.8×10^{17} and 1.64×10^{20} respectively.

C. Simulation Set 1 Results—Experimental Comparison

The results of the $N+/P$ diode single-event simulations for a laser energy of 13.5 pJ are compared to experimental data in Figs. 10 and 11. The simulation result using the proposed model agrees well with the measured data. Data for the experiment were only available up to 10^{-8} seconds due to the transient measurement setup [34]. As expected, the constant mobility model highly overpredicts mobility and causes a high current peak and charge collection. The simulation results using the proposed model fall between the Philips and Dorkel-Leturcq results. Since the initial maximum electron-hole pair concentration is just below 10^{18} cm^{-3} for the laser-strike, it follows that

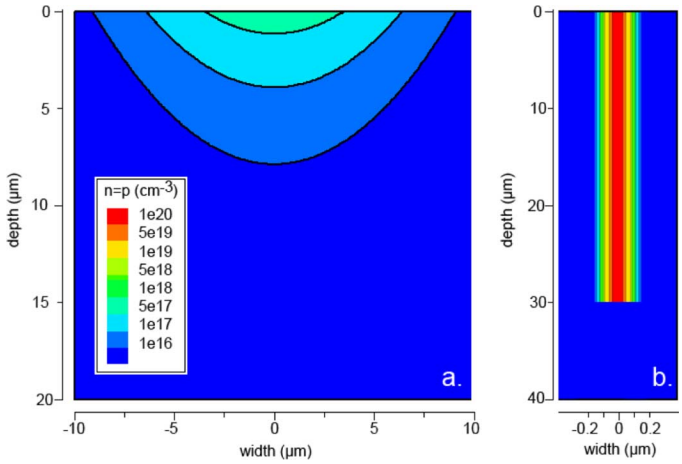

Fig. 9. Electron-hole pair distributions used in the simulations. (a) Single-photon absorption, laser energy = 13.5 pJ, radius = 6 μm [36], (b) Cylindrical Gaussian, LET = 20 MeV-cm^2/mg, 1/e radius = 50 nm.

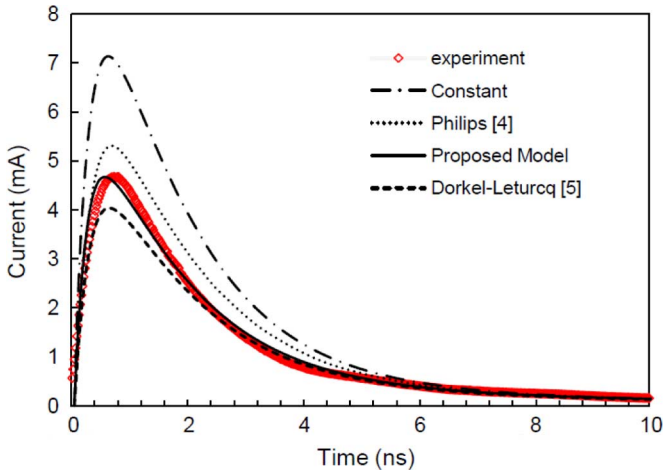

Fig. 10. Simulated laser-induced current transients in a reverse-biased Si N^+/P diode. Compared to experimental data for a laser energy of 13.5 pJ.

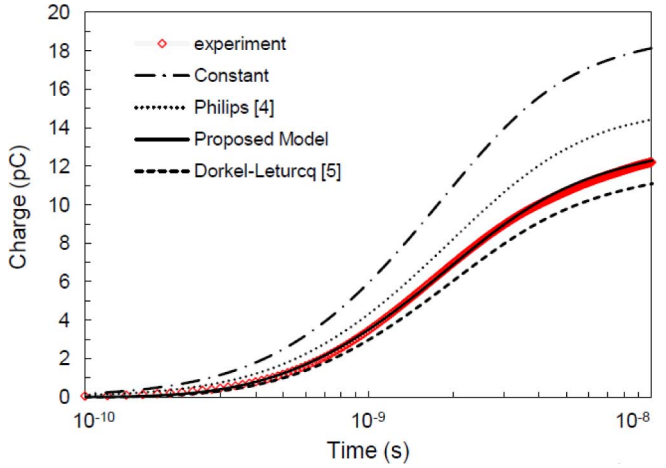

Fig. 11. FLOODS predicted charge collection in a reverse-biased Si N^+/P diode. Compared to experimental data for a laser energy of 13.5 pJ.

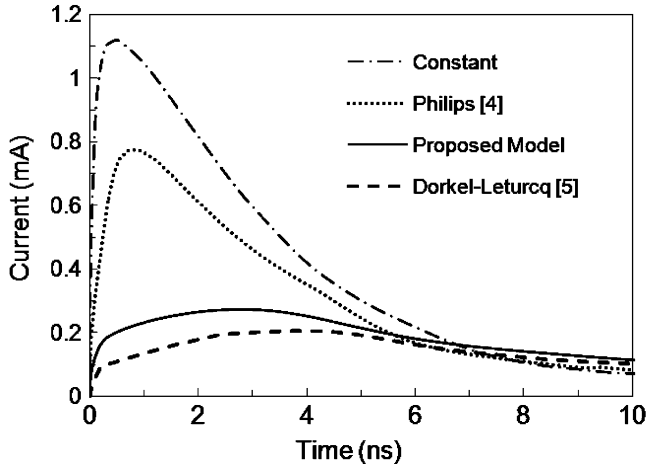

Fig. 12. Simulated current transients in a reverse-biased Si N^+/P diode. Strike track modeled by a cylindrical Gaussian, LET = 20 MeV-cm^2/mg.

the proposed model predicts a current transient and charge collection higher than the Dorkel-Leturcq model and less than the Philips model due to the high-injection mobility shown in Fig. 7.

D. Simulation Set 2 Results

Similar to the previous case, current transients on the N^+/P diode due to an ion strike were simulated to provide insight into the effects of higher injection levels. For this set, the cylindrical Gaussian profile in Fig. 9 was used instead of the laser SPA profile. The doping profile and structure are the same as in the previous simulation set. The simulation results of the current transient and charge collection are shown in Figs. 12 and 13. Understandably, the difference in results between the Philips model and the proposed model continues since the difference in high-injection mobility increases between the models at higher concentrations (Fig. 7). The Dorkel-Leturcq model still predicts lower charge collection compared to the proposed model. Since the Dorkel-Leturcq model underestimates doping dependent mobility (Figs. 2, 5, and 6) and predicts lower carrier-carrier mobility than the other models (Fig. 7), it follows that it results in lower charge collection than the other models.

E. Simulation Set 3 Results

Current transients for a $N^+/EPI/P^+$ diode were simulated using the cylindrical Gaussian ion charge deposition profile in Fig. 9. The diode structure consisted of a heavily doped n^+ region (10^{20} cm^{-3}) on a p-type epitaxial substrate (8×10^{14} cm^{-3}) placed on a p-type substrate (10^{20} cm^{-3}) and is similar to a structure reported in [37]. The n^+ junction depth was 0.1 μm and the p-type EPI layer was 5 μm thick. A 5 V reverse bias was applied to the device as in the previous simulations. The simulation results of the current transient and charge collection are shown in Figs. 14 and 15. Due to the much larger depletion region, the charge is collected more quickly than in the case of the bulk diode due to the strong drift region. Once

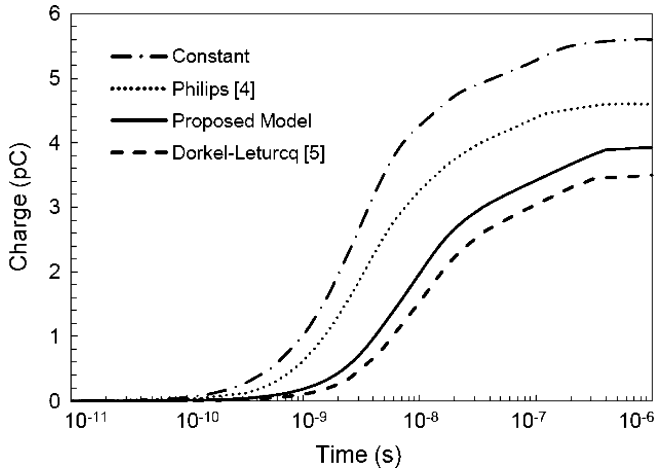

Fig. 13. FLOODS predicted charge collection for a reverse-biased Si N^+/P.

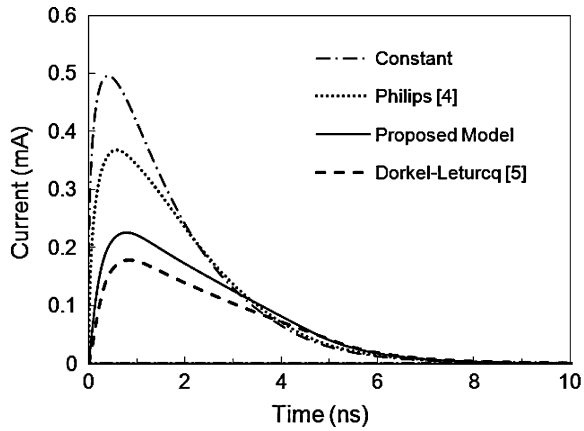

Fig. 14. Simulated current transients in a reverse-biased Si $N^+/EPI/P^+$ diode. Strike track modeled by a cylindrical Gaussian, LET $= 20$ MeV-cm^2/mg.

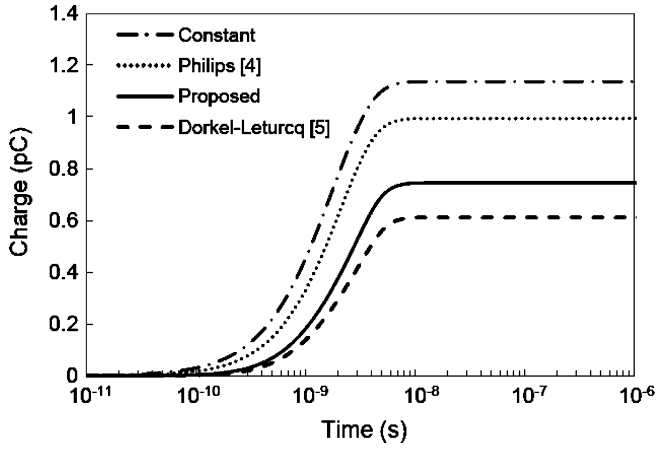

Fig. 15. FLOODS predicted charge collection for a reverse-biased Si $N^+/EPI/P^+$ diode.

again, the trend continues for charge collection where the simulation results using the proposed model fall between the Philips and Dorkel-Leturcq results.

F. Computational Comparison

The proposed model performed well in terms of computational efficiency. For example, in a 3-D $N+/P$ diode structure composed of $\sim$6000 volume elements, all device solution times were comparable when separately using each mobility model. The average sum of the matrix assembly and linear solution time was 9.66 seconds per Newton step for both the Dorkel-Leturcq model and the proposed model and 9.73 seconds per Newton step for the Philips model.

V. Conclusion

A comparison between existing mobility models for device simulation has been presented to discuss the particular advantages of each model, and a new model based on previous formulations is proposed that is computationally efficient and well suited to high injection conditions, such as those found in single-event simulation. As previously discussed, the proposed model has several advantages over the two most commonly used models for radiation effects simulations: the Philips unified mobility model and the Dorkel-Leturcq model. The Philips model is formulated in such a way such that it does not match known experimental data for electron and hole concentrations above 10^{17} cm^{-3}. The Dorkel-Leturcq model was not intended to account for doping concentrations of more than 10^{19} cm^{-3} and was not designed to fit minority mobility data. To address the disadvantages of these models, a new mobility model has been formulated to account for majority and minority carrier mobility, carrier-carrier scattering, and temperature dependence making it very suitable for both radiation effects simulations and general device simulations. Based on the simulation results of both laser and heavy-ion charge deposition using the various mobility models, the Philips and the Dorkel-Leturcq models provide "min-max" predictions for transient current and charge collection, whereas the proposed model provides an estimate, based on the best data currently available, which falls between these bounds. These simulation results indicate that the proposed mobility model gives a peak current, pulse width, and total charge collection for a single event simulation that is closer to experimental measurement than existing mobility models. To aid in mobility model fitting and parameterization, additional experimental data for cases where electron-hole carrier densities exceed 10^{18} cm^{-3} will be useful.

References

[1] P. Dodd and L. Massengill, "Basic mechanisms and modeling of single-event upset in digital microelectronics," *IEEE Trans. Nucl. Sci.*, vol. 50, pp. 583–602, 2003.

[2] J. C. Pickel, "Effect of CMOS miniaturization on cosmic ray-induced error rate," *IEEE Trans. Nucl. Sci.*, vol. NS-29, pp. 2049–2054, 1982.

[3] P. Dodd, F. Sexton, and P. Winokur, "Three-dimensional simulation of charge collection and multiple-bit upset in Si devices," *IEEE Trans. Nucl. Sci.*, vol. 41, pp. 2005–2017, 1994.

[4] D. Klaassen, "A unified mobility model for device simulation—I. Model equations and concentration dependence," *Solid State Electron.*, vol. 35, pp. 953–959, 1992.

[5] J. Dorkel and P. Leturcq, "Carrier mobilities in silicon semi-empirically related to temperature, doping and injection level," *Solid State Electron.*, vol. 24, pp. 821–825, 1981.

[6] G. Masetti, M. Severi, and S. Solmi, "Modeling of carrier mobility against carrier concentration in arsenic-, phosphorus-, and boron-doped silicon," *IEEE Trans. Electron Devices*, vol. 30, pp. 764–769, 1983.

[7] N. Arora, J. Hauser, and D. Roulston, "Electron and hole mobilities in silicon as a function of concentration and temperature," *IEEE Trans. Electron Devices*, vol. 29, pp. 292–295, 1982.

[8] D. Caughey and R. Thomas, "Carrier mobilities in silicon empirically related to doping and field," in *Proc. Inst. Electr. Eng.*, 1967, vol. 55, pp. 2192–2193.

[9] F. Dannhauser, "Dependence of carrier mobility in silicon on the concentration of free charge carriers-I," *Solid State Electron.*, vol. 15, pp. 1371–1375, 1972.

[10] J. Krausse, "Dependence of carrier mobility in silicon on the concentration of free charge carriers-II," *Solid State Electron.*, vol. 15, pp. 1377–1381, 1972.

[11] B. K. Ridley, *Quantum Process in Semiconductors*, 2nd ed. Oxford, U.K.: Clarendon, 1988, pp. 141–152.

[12] T. Zhang, "Impact of Charge Collection Mechanisms in Single Event Effects in SiGe HBT Circuits and Hardening Implications," M.S. thesis, Auburn Univ., Auburn, AL, 2009.

[13] A. Balasubramanian, "Measurement and Analysis of Single Event Induced Crosstalk in Nanoscale CMOS Technologies," Ph.D. dissertation, Vanderbilt Univ., Nashville, TN, 2008.

[14] P. Dodd, "Device simulation of charge collection and single-event upset," *IEEE Trans. Nucl. Sci.*, vol. 43, pp. 561–575, 1996.

[15] M. Fischetti, "Effect of the electron-plasmon interaction on the electron mobility in silicon," *Phys. Rev. B*, vol. 44, pp. 5527–5534, 1991.

[16] Synopsys, Sentaurus Device Manual, Oct. 2007, Version 2007.

[17] S. Li and W. Thurber, "The dopant density and temperature dependence of electron mobility and resistivity in n-type silicon," *Solid State Electron.*, vol. 20, pp. 609–616, 1977.

[18] S. Li, "The dopant density and temperature dependence of hole mobility and resistivity in boron doped silicon," *Solid-State Electron.*, vol. 21, pp. 1109–1117, 1978.

[19] P. Chapman, O. Tufte, J. Zook, and D. Long, "Electrical properties of heavily doped silicon," *J. Appl. Phys.*, vol. 34, pp. 3291–3295, 1963.

[20] D. Klaassen, "Physical modelling for bipolar device simulation," in *Proc. Conf. Simulation of Semiconductor Devices*, 1991, vol. 4, pp. 23–43.

[21] S. Swirhun, Y. Kwark, and R. Swanson, "Measurement of electron lifetime, electron mobility and band-gap narrowing in heavily doped p-type silicon," in *Proc. Int. Electron Devices Meeting*, Los Angeles, CA, 1986, pp. 2–5.

[22] J. Dziewior and D. Silber, "Minority-carrier diffusion coefficients in highly doped silicon," *Appl. Phys. Lett.*, vol. 35, pp. 170–, 1979.

[23] D. Tang, F. Fang, M. Scheuermann, T. Chen, and G. Sai-Halasz, "Minority carrier transport in silicon," in *Proc. Int. Electron Devices Meeting*, Los Angeles, CA, 1986, pp. 20–23.

[24] D. Burk and V. De La Torre, "An empirical fit to minority hole mobilities," *IEEE Electron Device Lett.*, vol. 5, pp. 231–233, 1984.

[25] S. Swirhun, J. D. Alamo, and R. Swanson, "Measurement of hole mobility in heavily doped n-type silicon," *IEEE Electron Device Lett.*, pp. 168–171, 1986.

[26] C. Wang, K. Misiakos, and A. Neugroschel, "Minority-carrier transport parameters in n-type silicon," *IEEE Trans. Electron Devices*, vol. 31, pp. 1314–1322, 1990.

[27] C. Choo, "Theory of a forward-biased diffused-junction PLN-rectifier: Part I," *IEEE Trans. Electron Devices*, vol. 19, pp. 954–966, 1972.

[28] S. M. Sze, *Physics of Semiconductor Devices*. New York: Wiley, 1981.

[29] J. R. Meyer and M. Glicksman, "Electrical conductivity of germanium as a function of optically injected carrier density and temperature," *Phys. Rev. B*, vol. 17, no. 8, pp. 3227–3238, 1978.

[30] J. S. Laird, S. Onoda, and T. Hirao, "Relaxation of high-energy heavy-ion induced bipolar plasmas in Si epilayer devices as a function of temperature," *J. Appl. Phys.*, vol. 104, p. 084510, 2008.

[31] C. Lombardi, S. Manzini, A. Saporito, and M. Vanzi, "A physically based mobility model for numerical simulation of nonplanar devices," *IEEE Trans. Comput.-Aided Design Integr. Circuits Syst.*, vol. 7, pp. 1164–1171, 1988.

[32] M. Darwish, J. Lentz, M. Pinto, P. Zeitzoff, T. Krutsick, and H. Vuong, "An improved electron and hole mobility model for general purpose device simulation," *IEEE Trans. Electron Devices*, vol. 44, pp. 1529–1538, 1997.

[33] C. Canali, G. Majni, R. Minder, and G. Ottaviani, "Electron and hole drift velocity measurements in silicon and their empirical relation to electric field and temperature," *IEEE Trans. Electron Devices*, vol. 22, pp. 1045–1047, 1975.

[34] H. Park, D. J. Cummings, R. Arora, J. A. Pellish, R. A. Reed, R. D. Schrimpf, D. McMorrow, S. E. Armstrong, U. Roh, T. Nishida, M. E. Law, and S. E. Thompson, "Laser-induced current transients in strained-Si diodes," *IEEE Trans. Nucl. Sci.*, vol. 56, pp. 3203–3209, 2009.

[35] M. E. Law, FLOODS/FLOOPS Manual, Univ. Florida, Gainesville, FL, 2009, Available: [Online]. Available: http://www.flooxs.ece.ufl.edu

[36] D. McMorrow, W. T. Lotshaw, J. S. Melinger, S. Buchner, and R. L. Pease, "Subbandgap laser-induced single event effects: Carrier generation via two-photon absorption," *IEEE Trans. Nucl. Sci.*, vol. 49, pp. 3002–3008, 2002.

[37] L. D. Edmonds, "Charge collection from ion tracks in simple EPI diodes," *IEEE Trans. Nucl. Sci.*, vol. 44, pp. 1448–1463, 1997.